AIMS Energy, 10(5): 987–1004.
DOI: 10.3934/energy.2022045
Received: 10 February 2022
Revised: 25 June 2022
Accepted: 25 July 2022
Published: 2 September 2022

http://www.aimspress.com/journal/energy

Research article

Ant colony optimization algorithm and fuzzy logic for switched reluctance generator control

Rabyi Tarik* and Brouri Adil

L2MC laboratory, SECNDCM teams, ENSAM, Moulay Ismail University, 50000 Meknes, Morocco

* **Correspondence:** Email: tarikensam@yahoo.fr; Tel: +212535467160.

Abstract: This article discusses two methods to control the output voltage of switched reluctance generators (SRGs) used in wind generator systems. To reduce the ripple of the SRG output voltage, a closed-loop voltage control technique has been designed. In the first method, a proportional-integral (PI) controller is used. The parameters of the PI controller are tuned based on the voltage variation. The SRG is generally characterized by strong nonlinearities. However, finding appropriate values for the PI controller is not an easy task. To overcome this problem and simplify the process of tuning the PI controller parameters, a solution based on the ant colony optimization algorithm (ACO) was developed. To settle the PI parameters, several cost functions are used in the implementation of the ACO algorithm. To control the SRG output voltage, a second method was developed based on the fuzzy logic controller. Unlike several previous works, the proposed methods, ACO and fuzzy logic control, are easy to implement and can solve numerous optimization problems. To check the best approach, a comparison between the two methods was performed. Finally, to show the effectiveness of this study, we present examples of simulations that entail the use of a three-phase SRG with a 12/8 structure and SIMULINK tools.

Keywords: switched reluctance generator; PI controller; wind generator systems; ant colony optimization; fuzzy logic control

1. Introduction

Over the years, the switched reluctance generator (SRG) has been a focal point for many research

studies [1]. The SRG has a basic, rigid and simple structure. This device includes neither a permanent magnet nor twisting of the rotor. This construction decreases thus the expense of the SRG and its maintenance. The SRG can operate during high-velocity activities without the worry of mechanical problems [2].

Accordingly, the SRG offers several advantages compared to other machines, e.g., the rotor does not require any winding and it is constituted only of ferromagnetic material. The major windings (losses) are concentrated in the stator. There are numerous sorts of structures that can drive the SRG [3]. The power electronic converter usually used for controlling the SRG is the asymmetric power electronic converter. It has the advantage of being able to independently control each phase of the SRG [4]. The stator windings are associated with the arrangement of the upper and lower switches of the inverter [5]. Due to the complex nonlinear characteristics of SRGs, there exist very few previous works dedicated to the identification and modeling of SRGs [6,7]. This was later described as nonlinear systems structured in blocks [8–10]. The most popular models of nonlinear systems in blocks can be found in [11–13]. The system nonlinearities can be static or dynamic [14–16]. Note that the problem of SRG speed control has been addressed by using several techniques, e.g., fuzzy logic control [17], artificial neural networks (ANNs) [18] and genetic algorithms [19,20]. Furthermore, the optimization techniques like particle swarm optimization and bacteria foraging can be used to regulate the SRG speed. Then, an ANN-proportional integral (ANN-PI) controller was introduced to regulate the power injected into the grid [21]. A proportional resonant controller that has been used to control the power produced by the SRG is given in [22]. To minimize the torque ripple of SRGs, an ANN control method has been developed, as presented in [23]. To control the position of the linear switched reluctance machine, a flower pollination algorithm was developed [24].

The fuzzy logic technique was introduced by Zadeh in 1965 [25]. The fuzzy logic controller (FLC) has been widely investigated and used to regulate complex nonlinear systems. The FLC is an artificial decision-maker that relies on human decision-making behavior through the use of language rules rather than mathematical models [26]. An exact model is not necessarily required with the FLC technique and it is created using language information. Mathematical equations to describe the system to be controlled are not necessary for FLCs. The FLC has been used in many fields, e.g., in solar photovoltaic systems [27], wind energy [28], power systems [29] and smart agriculture systems [30]. Other previous works have yielded combinations of fuzzy logic with other methods. In [31], the authors used an adaptive neuro-fuzzy inference system to assist the power monitoring for a smart grid. Adaptive fuzzy control using a genetic algorithm has been used to overcome the influence of nonlinearities in the vessel dynamic positioning system [32]. In [33], a self-tuning FLC-based speed is proposed for the control of an SRG for wind energy applications. The ACO is a heuristic approach that can be used to find the global optimum of a given problem. In this respect, note that the ACO has already been employed in wind energy control [34] and for planning the wind farm layouts [35]. In [36], the authors discussed a design method entailing the use of the ACO based on a proportional-integral-derivative (PID) controller for a zeta converter.

The aim of this study was to control the output voltage of the SRG. Techniques using the ACO-based PI controller and FLC have been developed. In this respect, the SRG output voltage is adjusted by using the turn-off angle θ_{off}. To obtain the best value of θ_{off}, two methods are proposed. The first one consists of a PI controller tuned by an ACO algorithm. In the second approach, the tun-off angle θ_{off} is determined by using an FLC.

For convenience, the main contributions of this work are summarized as follows:

- Unlike many previous methods dedicated to controlling the SRG voltage, the proposed methods are easy to implement.
- In this paper, very interesting tools and concepts are proposed, such as ACO for tuning the PI controller, as well as the FLC approach.
- The established algorithm, which applies an ACO technique for SRG voltage control, is new.
- To improve the results obtained via the ACO algorithm, four cost functions were applied and compared.
- In this study, a second solution to control the SRG output voltage by implementing a FLC approach was also developed. The best solution was chosen by comparing these two methods.

The paper is organized as follows. The mathematical model and operation principle of SRGs are introduced in Section 2. In Section 3, the control methods for the SRG based on the ACO and FLC are described. An overview and description of the ACO are presented. Then, the cost functions used to optimize the ACO method are also proposed in this section. Then, the FLC is discussed. To show the effectiveness of these methods, simulation examples are presented in Section 4. Finally, comparisons between the results obtained using the two approaches are also discussed in this section. In Section 5, the concluding remarks of this paper are summarized.

2. Mathematical model and operation of SRGs

2.1. Mathematical model of the SRGs

First, note that the SRG winding flux $\lambda(.)$ depends on the phase current i and the rotor position θ. Then, for each stator phase, the voltage v can be expressed as the sum of the voltage drop on the resistor and the derivative of the flux:

$$v = R_s i + \frac{d\lambda(\theta,i)}{dt} \tag{1}$$

where R_s is the phase resistor. The phase inductance $L(\theta, i)$ is a nonlinear function depending on the rotor position θ and the phase current i. Furthermore, the linkage flux $\lambda(\theta, i)$ can be expressed according to L and i as follows:

$$\lambda(\theta, i) = L(\theta, i)i \tag{2}$$

Then, replacing the flux $\lambda(\theta, i)$ in Eq (2) with its expression according to L and i, the expression of phase voltage becomes

$$v = R_s i + L(\theta, i)\frac{di}{dt} + i\frac{d\theta}{dt}\frac{\partial L(\theta,i)}{\partial \theta} \tag{3}$$

The last term on the right side of Eq (3) corresponds to the back electromotive force e. Specifically, one has

$$e = i\frac{d\theta}{dt}\frac{\partial L(\theta,i)}{\partial \theta} = i\omega\frac{\partial L(\theta,i)}{\partial \theta} \tag{4}$$

where ω is the SRG's rotor speed. When the SRG operates as a generator, the current changes its direction. The back electromotive force thus becomes negative.

2.2. Operation principle of SRGs

The SRG stator is characterized by winding resistors with very small values [6]. The resistive voltage drop can be neglected [6]. Accordingly, the phase current i, the phase voltage, v and the back electromotive force e are related by the following equation:

$$v - e = L(\theta)\frac{di}{dt} \tag{5}$$

Here, an asymmetric half-bridge (AHB) converter is proposed to drive the SRG (Figure 1). The SRG operates as a generator when the phase inductance $L(\theta)$ decreases; this means that $dL\,(\theta)/dt < 0$ (Figure 2).

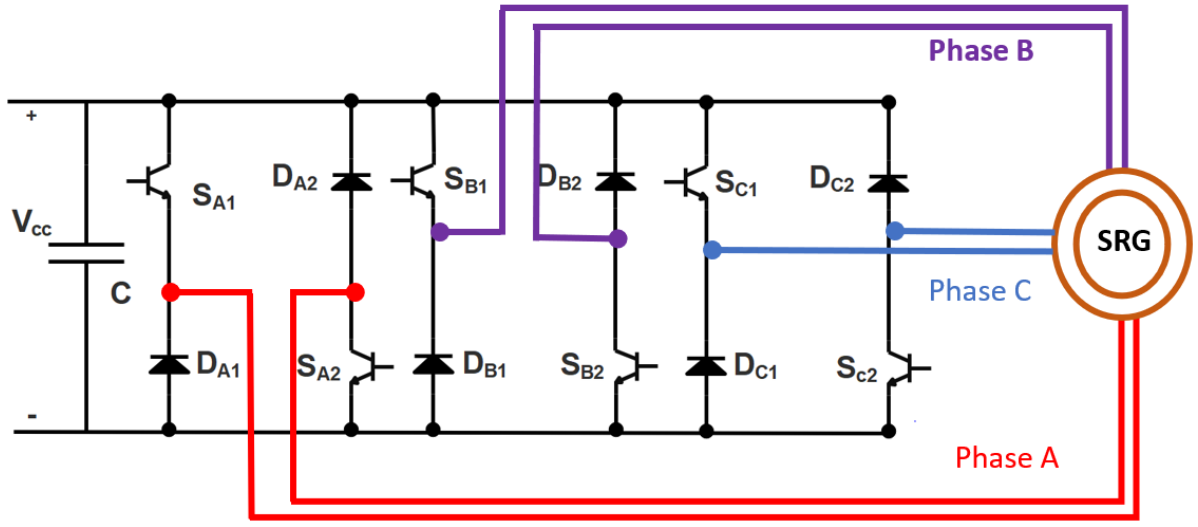

Figure 1. SRG connected to an AHB converter.

The SRG is interconnected via the DC link to a voltage source converter (VSC), which is linked to the electrical grid. Then, the DC link voltage V_{DC} is regulated by the VSC control. The latter allows for the injection of the generated power from the SRG into the electrical grid.

In this respect, note that the characteristics $L(\theta)$ and $i(\theta)$ are smooth curves and are often linearized in the study of generator and motor modes of SRGs, as shown in Figure 2 [37]. It can be easily seen in Figure 2 that the curve of the electrical current i can be subdivided into three main intervals, or the following three situations:

- The first situation is characterized by $e < V_{DC}$. In this case, the phase current decreases after the excitation stage. This situation happens when the operating speed is decreased due to the electromotive force diminishing.
- The second situation can be obtained when $e = V_{DC}$. Accordingly, after the duration of the excitation stage, the current tends to remain constant.
- The last situation can be seen when the SRG is working at high speeds; one thus has $e > V_{DC}$. After the excitation stage, the phase current tends to rise.

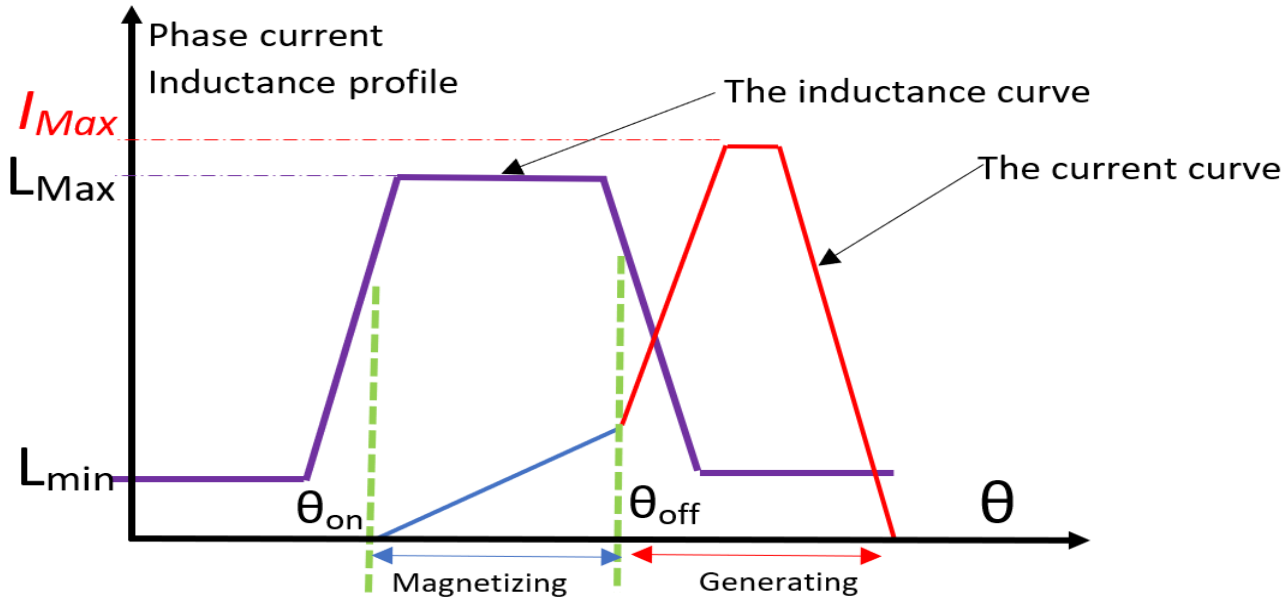

Figure 2. Excitation and generation stages for one SRG phase.

To determine the SRG's operation mode, the base speed should be evaluated. To improve the SRG performance, two techniques for SRG control can be used. For low operating speeds, the control of the SRG is performed by using the existing hysteresis method. The power control of the SRG is related to the adjustment of the reference current I_{ref}. In this respect, the firing angle θ_{on} and turn-off angle θ_{off} are the driving parameters (Figure 2). For high speeds, the control of the SRG is achieved by using a single-pulse technique. Accordingly, the power control is based on changing the turn-off angle θ_{off} while the firing angle θ_{on} is kept constant.

3. Control method for SRGs: ACO and FLC

3.1. ACO technique

3.1.1. Overview and description of the ACO algorithm

ACO is a meta-heuristic algorithm and probabilistic method. It is commonly used for solving hard combinatorial optimization problems based on graph representations. This method aims to find the best paths based on several possible graphs. This algorithm was initially proposed by Marco Dorigo in 1992 [38]. The artificial ants used in this technique were inspired by real ant colonies and designed to search for the best path. The shorter path is obtained by analyzing and combining the results of the path of each ant in the colony. The main issue is related to finding the shortest path among all of the trajectories traveled by different ants to reach the food. When the ants are moving, they leave a chemical pheromone trail on the ground. Depending on the distance of the path, the pheromone quality will change. Every ant chooses the path according to the intensity of the deposited pheromone. If there is no more deposit of pheromone, its intensity decreases according to the time. Specifically, the other ants are attracted by the pheromone; they thus choose the path where the pheromone is of high intensity. This path will be the best solution and has a great probability of being chosen.

With this approach, the lifestyle behavior of real ant colonies is used to solve the optimization problem. Here, the artificial ant technique is proposed to seek the best solution by moving from one node to another. With this algorithm, the artificial ants move according to their previous positions, which have been stored in a specific data structure. Once the ants have accomplished their tour between the initial node and the last one, the pheromone consistency of each path is updated. The concentration of pheromone will be of high quality if the artificial ants finished their tour by taking the shortest path, and vice versa. The steps of the proposed algorithm are summarized in Figure 3.

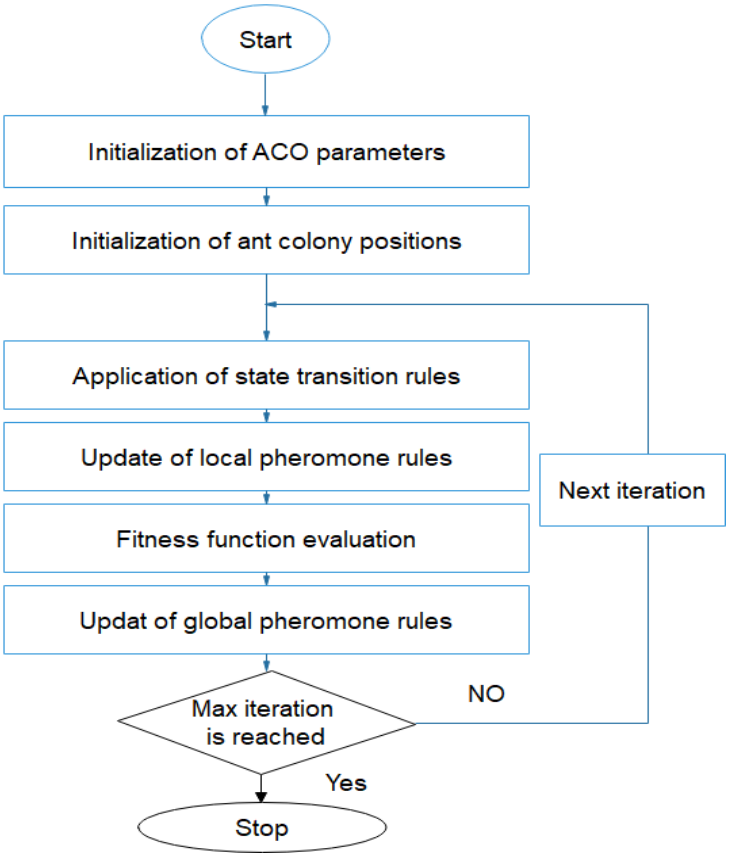

Figure 3. ACO algorithm.

3.1.2. Cost functions and objective function for the ACO technique

For problem optimization, there are several error criteria commonly used in the literature, including the integral square error (ISE), integral of the absolute error (IAE), integral time of the absolute error (ITAE), integral of multiplied absolute error, quadratic error and total square variation. All of these error criteria have zero as the lower bound and can be considered as cost functions of the proposed ACO algorithm. To improve the overall performance obtained through the use of the PI controller, four cost functions were selected. The considered cost function criteria are ISE, mean squared error (MSE), IAE and ITAE. Specifically, the objective function of the ACO algorithm is based on minimizing the considered error criteria. The parameters of the PI controller can be obtained by using the optimization results.

3.1.3. Closed-loop control of SRGs via ACO

Here, the ACO-based control method for the SRG voltage is introduced. Figure 4 shows the closed-loop control corresponding to this technique, where V_{ref} denotes the reference voltage and V_m stands for the SRG output voltage. With this method, the SRG is driven at high speeds. The firing angle θ_{on} is kept constant at 40°, while the turn-off angle θ_{off} is adjusted by the algorithm. Accordingly, the magnetization cycle of the SRG phase is controlled by changing the value of θ_{off} through the use of a PI controller.

Even if the PID controller would improve the system stability, the derivative action of the PID controller would likely increase the amplitude of disturbances. Furthermore, a couple of ripples is often produced in SRG applications. In order to avoid more disturbances, a PI controller was selected.

In the proposed approach, the PI controller parameters are obtained by using an ACO algorithm. The transfer function of the proposed PI controller is as follows:

$$G_c(S) = K_P + \frac{K_I}{S} \tag{6}$$

where K_P and K_I are parameters of the PI controller.

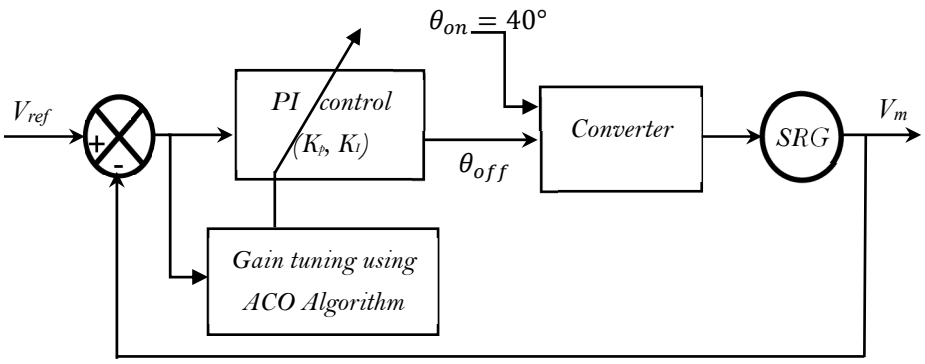

Figure 4. SRG voltage control via PI controller implementation in ACO.

3.2. FLC

3.2.1. Description of the FLC

Generally, the FLC has three main stages, namely, fuzzification, fuzzy rule extraction and defuzzification. The inputs are turned into fuzzy sets by using linguistic elements and membership functions throughout the fuzzification process. The two most well-known fuzzy systems are the Mamdani and the Takagi-Sugeno-Kang models. Here, the Mamdani fuzzy systems have two inputs and one output is used. The voltage error signal ε ($\varepsilon = V_{ref} - V_{out}$) and its derivative $\dot{\varepsilon}$ are the inputs of the FLC. The output θ_{FLC} of the FLC corresponds to the turn-off angle θ_{off} of the SRG.

The design of the FLC was determined by assigning seven fuzzy sets for the inputs (ε, $\dot{\varepsilon}$) and the output (θ_{FLC}), namely, {NB (negative big), NM (negative middle), NS (negative small), ZZ (zero), PS (positive small), PM (positive middle), PB (positive big)}. In this study, the membership functions related to (ε, $\dot{\varepsilon}$) and θ_{FLC} are the chosen type of triangular shapes; they are given by Figure 5 and Figure **6**,

respectively.

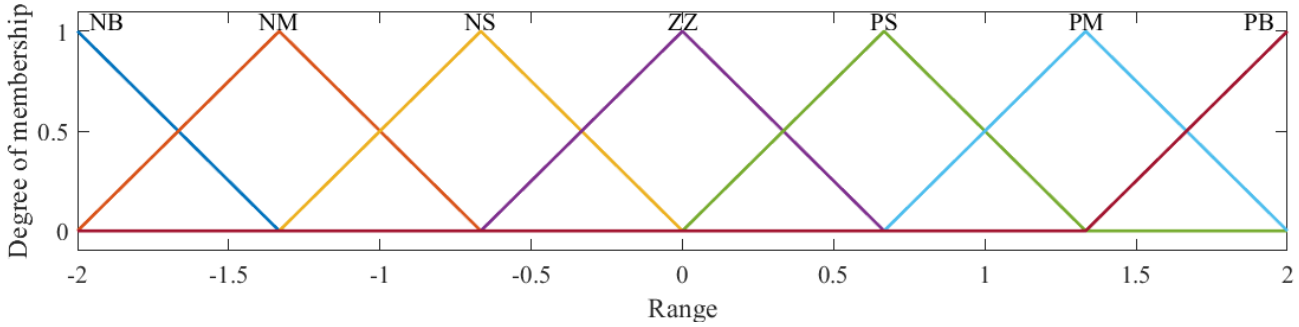

Figure 5. Membership functions corresponding to the inputs ε and $\dot{\varepsilon}$.

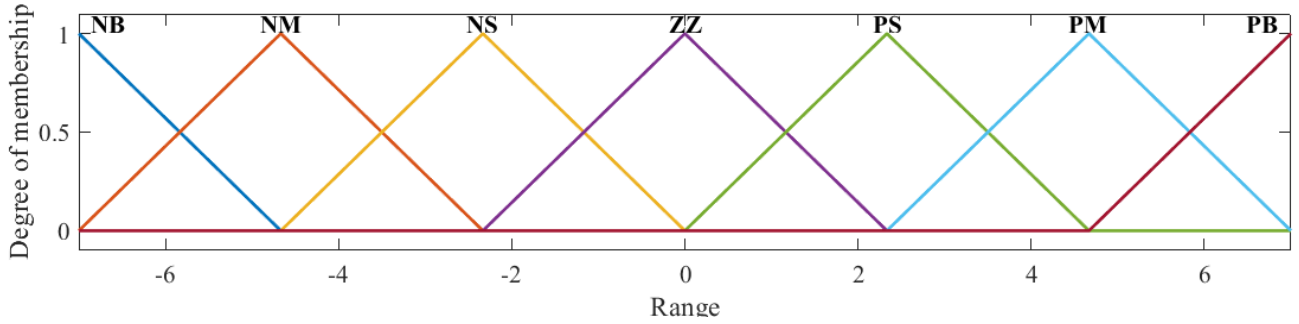

Figure 6. Membership functions corresponding to the output θ_{FLC}.

3.2.2. Closed-loop control of SRG through the use of an FLC

The second method developed in this work consists of using an FLC to determine the best values of θ_{off} while the angle θ_{on} is fixed at 40°. Figure 7 shows the closed-loop control corresponding to this technique.

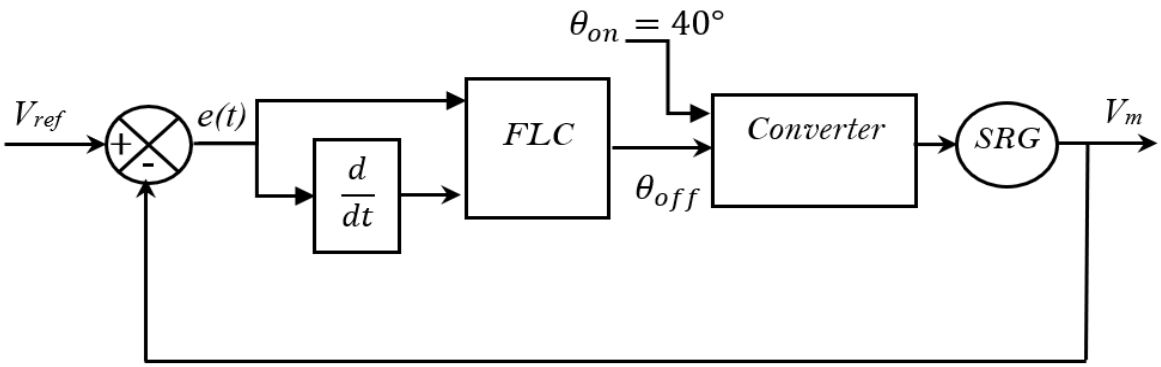

Figure 7. SRG voltage control through the use of fuzzy logic.

4. Simulation results and discussion

In this section, examples of simulations are presented to show the effectiveness of the proposed

methods. The first method aims to control the output voltage of the SRG by using an ACO algorithm. This method has two steps. In the first step, the optimum parameters for each cost function (i.e., ISE, MSE, IAE and ITAE) of the PI controller are determined. The optimum PI controller parameters are chosen by taking the parameter values that yields the smallest error between the reference voltage and the output voltage of the SRG. In the second step, the obtained values are compared based on the time domain specifications. Specifically, the steady-state time, peak time and overshoot.

In the second method, an FLC replaces the PI controller.

Remark 1:

The applied SRG is characterized by the parameters given in the Appendix (Part a). The initialization parameters of the ACO algorithm and PI controller are also given in the Appendix (Parts b and c).

The approach used to initialize the ACO algorithm is based on results reported in the literature and simulations. First, we applied many combinations by changing the number of ants (10, 20, 30, 40, 50, 80) and the number of iterations (20, 50, 100, 200) in simulations. Second, in consideration of the obtained results and time constraints, we have chosen the optimal number of ants as 30 and optimal number of iterations as 100.

4.1. System response when using the PI controller

Based on the ACO algorithm, the parameters for the optimal PI controllers corresponding to each cost function were obtained; they are presented in Table 1.

Table 1. Optimal PI parameters for each cost function.

ACO	K_P	K_I
ITAE	0.36977	2.497
MSE	2.7879	5.8634
IAE	1.802	0.82332
ISE	1.2821	4.7698

The responses of the SRG output voltage corresponding to the use of the optimal PI controllers have been plotted as shown in Figure 8 and Figure 9, where the reference voltage is constant ($V_{ref} = 400\ V$). The error variations for the ISE, IAE, MSE and IATE have been plotted as shown in Figure 10, Figure 11, Figure 12 and Figure **13**, respectively.

To compare the performances of the PI controllers, their characteristic time-domain specifications (steady-state time, peak time, overshoot) were compared; the results are given in Table 2. Finally, the best PI controller was chosen. For convenience, the voltage ripple of the output voltage signal resulting from the use of the ACO-PI controller method and the cost error ITAE was estimated. The value of this voltage ripple was 0.76%.

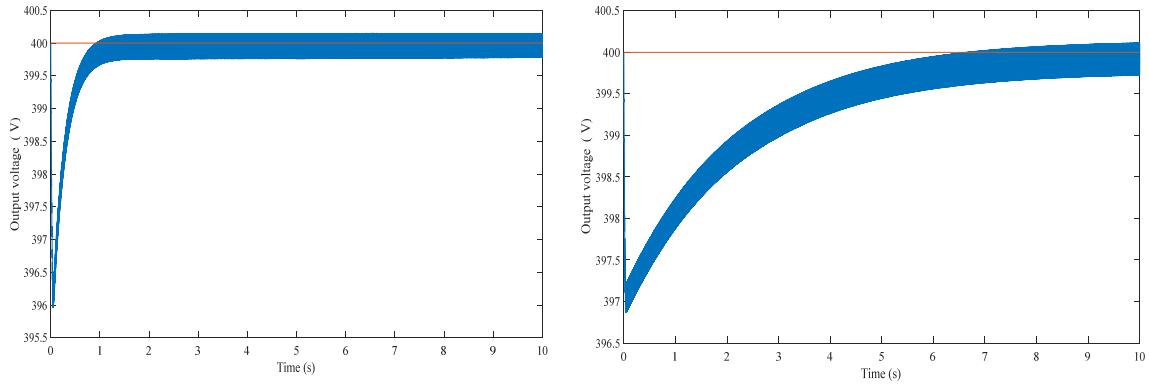

(a) (b)

Figure 8. Output voltage and voltage reference based on ISE (a) and IAE (b).

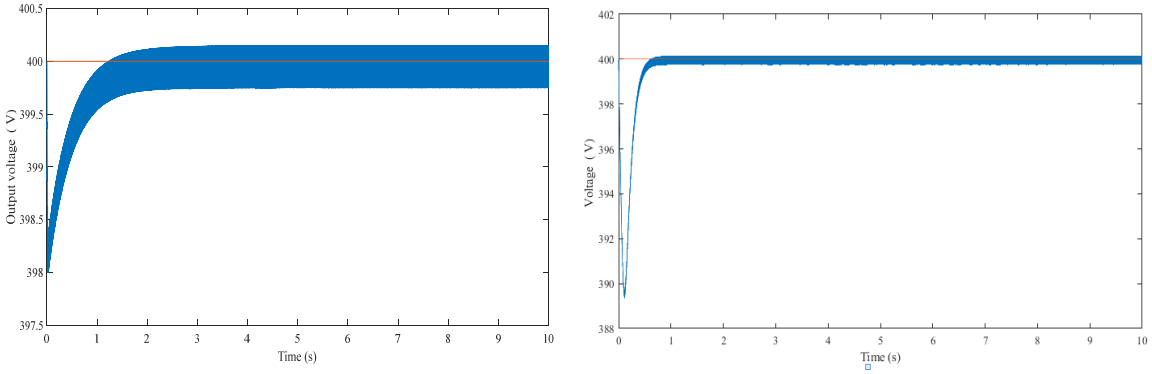

(a) (b)

Figure 9. Output voltage and voltage reference based on MSE (a) and ITAE (b).

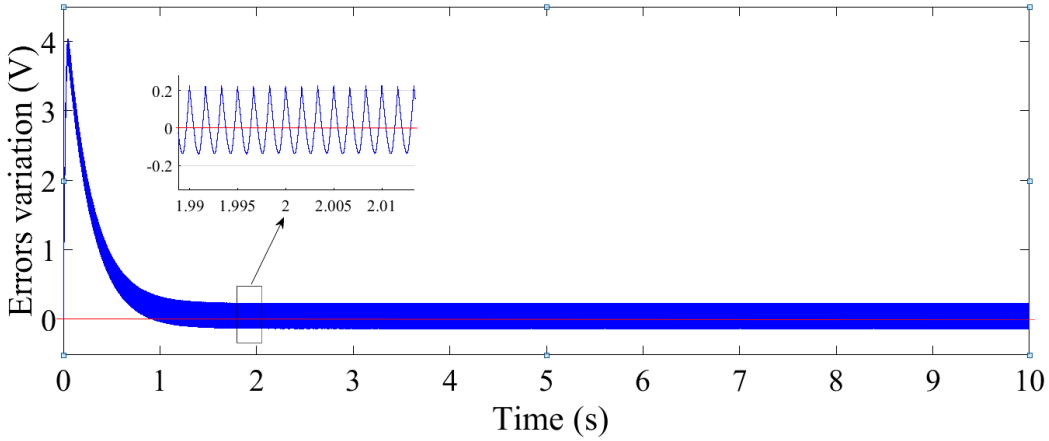

Figure 10. Error variation for ISE.

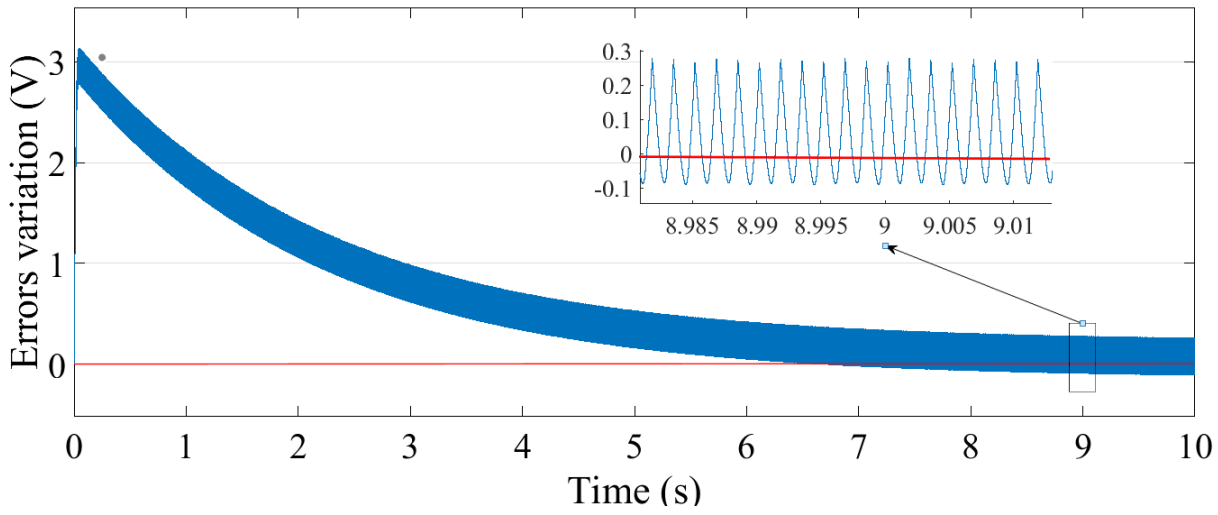

Figure 11. Error variation for IAE.

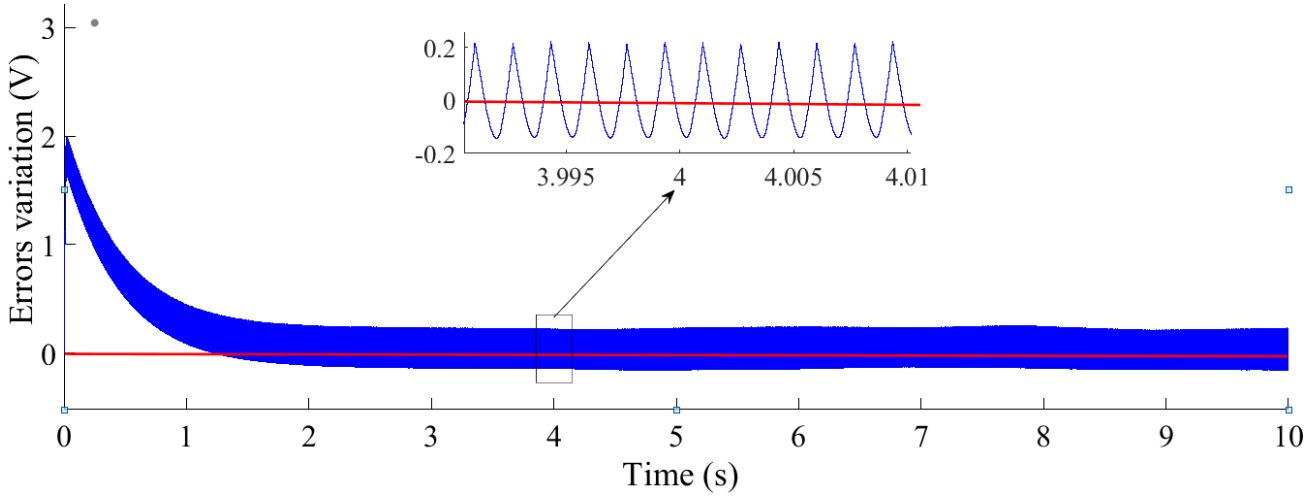

Figure 12. Error variation for MSE.

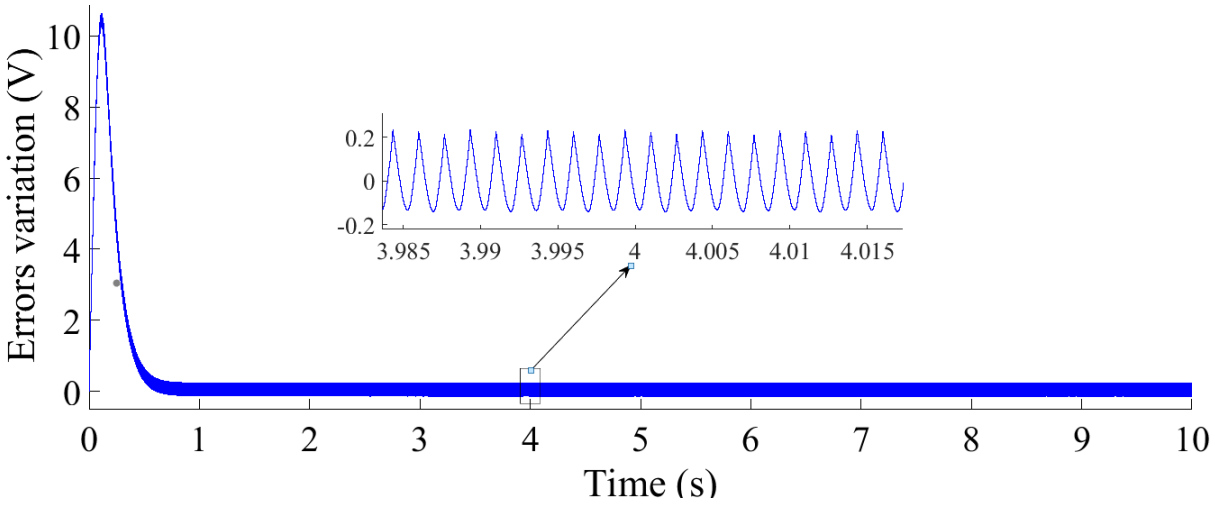

Figure 13. Error variation for ITAE.

4.2. System response when using the FLC

In the second method, the PI controller is replaced with an FLC. In this respect, two cases can be distinguished. The first one consists of taking the wind speed as constant; in the second case, the wind speed is variable. When the wind speed is taken as a constant (here, $\omega = 157\,rad/s$), the response of the output voltage of the SRG as a result of using the FLC was determined; it is shown in Figure 14; the error variation is shown in Figure 15. The results obtained for the time domain are summarized in Table 2. It can be seen that the output voltage signal of the FLC yields a voltage ripple with a value of 0.54%.

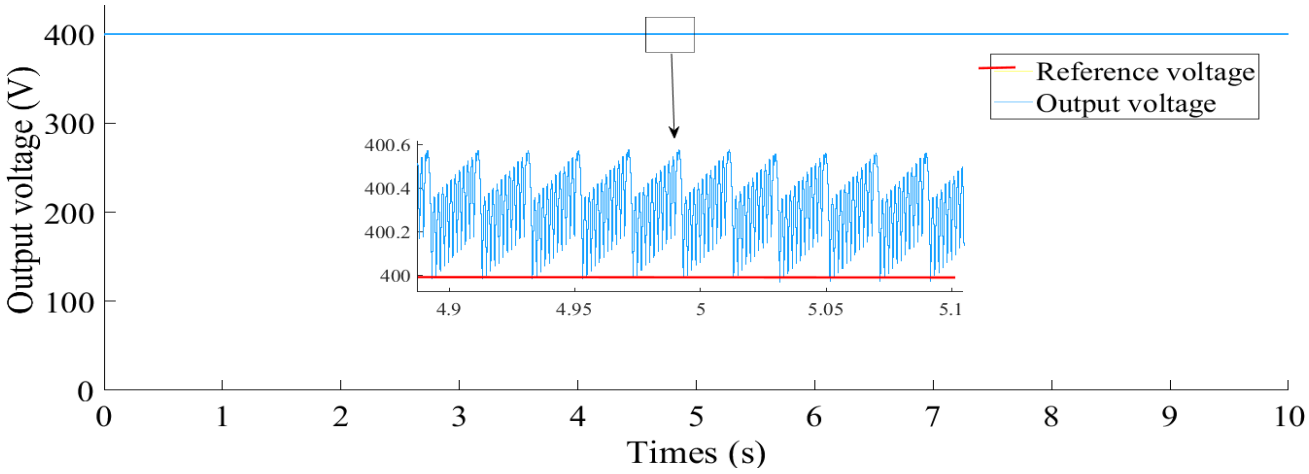

Figure 14. Output voltage obtained by using an FLC with ω = 157 rad/s and V_{ref} = 400 V.

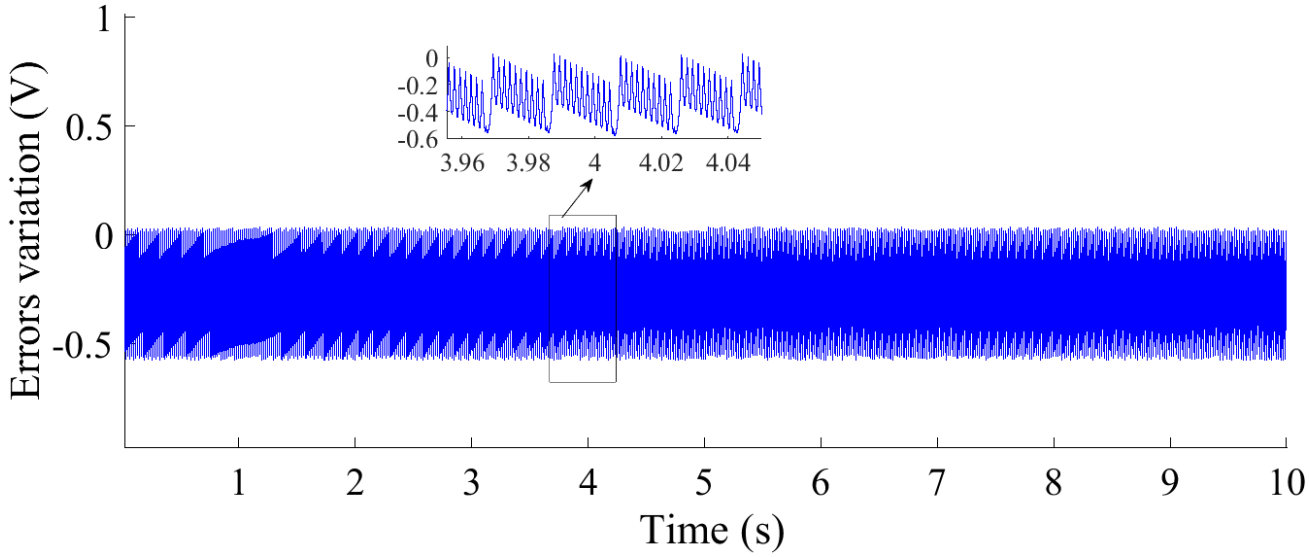

Figure 15. Error variation resulting from operating the FLC with ω = 157 rad/s and V_{ref} = 400 V.

Table 2. Time-domain characteristics of the output voltage according to the control method.

Method	Cost function type	Peak time	Peak	Undershoot	Overshoot	Settling max	Settling min	Settling time	Rise time
PI	ACO-ITAE	5.5277	400.1517	0	0.0015	400.1517	399.7504	9.9993	0.4553
PI	ACO-MSE	8.2291	400.1502	0	2.4386e-04	400.1502	399.7400	9.9997	1.2306
PI	ACO-IAE	9.9650	400.1138	0	1.4018e-04	400.1138	399.7126	9.9997	2.4563
PI	ACO-IAE	9.9650	400.1138	0	1.4018e-04	400.1138	399.7126	9.9997	2.4563
FLC	--------	*****	400.8519	0	0.0596	400.8519	399.7932	*****	******

Here, the wind speed was varied from $110\,rad/s$ to 170 rad/s. The wind speed curve is given in Figure 16. For this case, the SRG output voltage corresponding to the use of the FLC controller can be seen in Figure 17; the error variation is shown in Figure 18.

The characteristics of the SRG output voltage signal corresponding to the ACO-PI control scheme with IATE, as well as that corresponding to the FLC scheme are summarized in Table 3.

Table 3. Characteristics of the SRG output voltage signal based on ACO-PI-IATE and FLC implementation.

Output voltage	ACO-PI-ITAE	FLC
Max	4.002e + 02	4.006e + 02
Min	3.960e + 02	4.000e + 02
Peak to peak	4.190e + 00	6.123e 01
Mean	3.999e + 02	4.003e + 02
Median	4.000e + 02	4.003e + 02
Root-mean-square	3.999e + 02	4.003e + 02

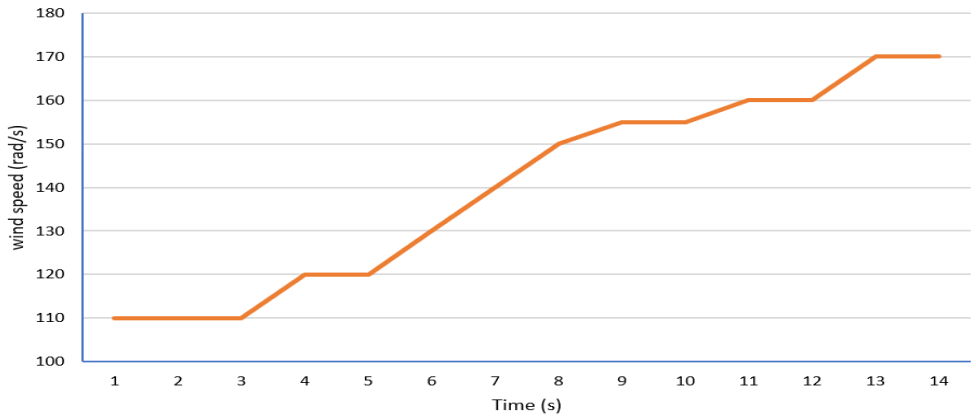

Figure 16. Profile of wind speed.

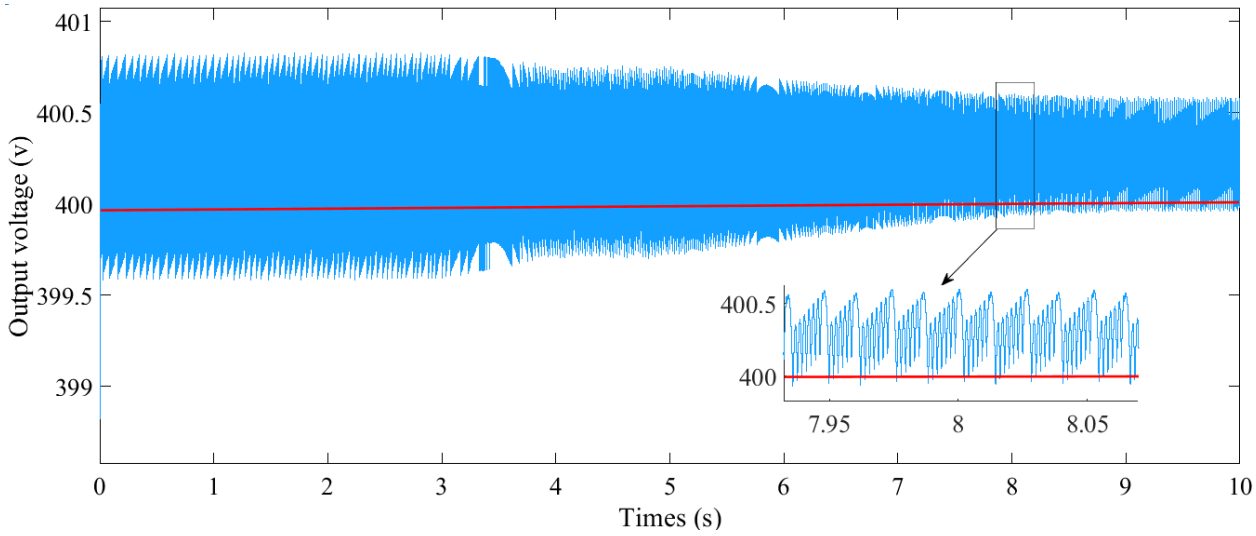

Figure 17. Output voltage resulting from implementation of the FLC with variable wind speed.

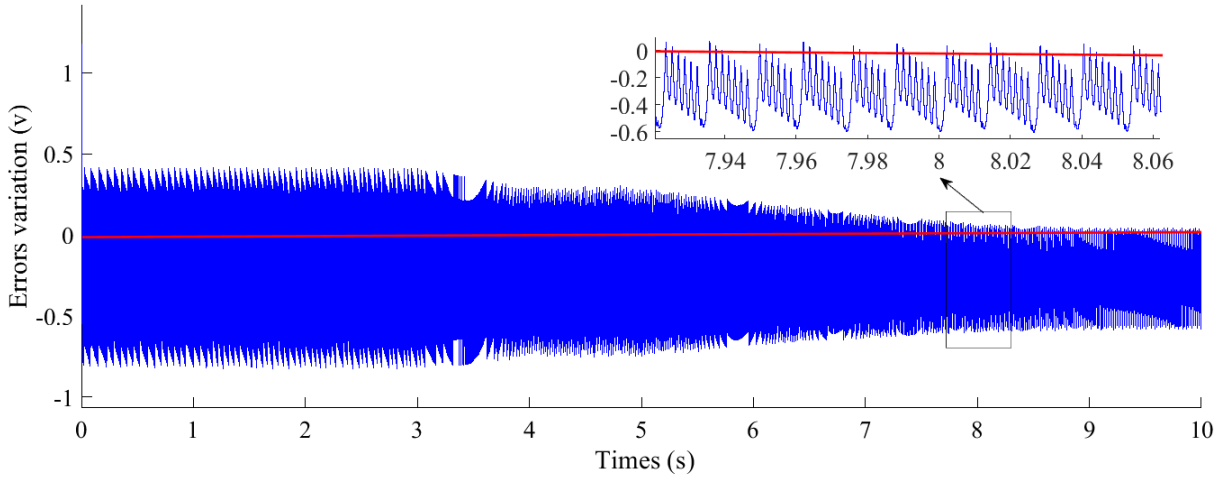

Figure 18. Error variation associated with the FLC and the condition of variable wind speed.

4.3. Results and discussion

- Case of constant wind speed

To show the effectiveness of this study, examples of simulations have been provided. The reference voltage was kept constant at $V_{ref} = 400\ V$. These simulations were established by applying a constant wind speed of $157\ rad/s$ and choosing a load of 1600 Ω. The results of the SRG output voltage that were obtained by using a conventional PI controller with different cost functions (i.e., ACO-ISE, ACO-MSE, ACO-IAE and ACO-ITAE), and as based on fuzzy control, are shown in Figures 8, 9 and 14. These results show that the SRG output voltage resulting from the use of the ACO-based PI controller and the FLC techniques converges to its reference value. It can be seen by using this method that a constant torque allows a constant voltage. On the other hand, the results summarized in Table 2 show that the ACO-based PI controller that utilizes ITAE provides the best results. Additionally, the time-domain characteristics show that the FLC improves the dynamic and steady-state features. Furthermore, the FLC yielded a smaller voltage ripple (0.54%) than the PI controller (0.76%).

- Case of variable wind speed

The wind speed was varied in the range of 110–170 rad/s. The proposed simulations were established by taking the reference voltage $V_{ref} = 400\ V$ and applying a load of 1600 Ω. Generally, the tuning of the ACO-based PI controller parameters requires significant computational time. Thus, to overcome this issue, an FLC controller was developed. It is shown in Figure 17 that the SRG output voltage converges fast to the reference voltage even if the wind speed changes.

5. Conclusions

This article discusses the problem of SRG output voltage control. This SRG was implemented in a wind turbine operating at 75 KW that was connected to an electrical grid. Here, a PI controller based on the ACO technique has been proposed to regulate the SRG output voltage. To determine the PI controller parameters, several cost functions were used. By comparing the different results obtained by using the given cost functions, the best PI controller parameters were chosen.

When the wind speed was taken as constant, the simulation results confirmed that the output voltage associated with the ACO-PI controller technique and a cost function (i.e., ITAE, MSE, IAE or ISE) converges to the reference voltage. Furthermore, it has been shown that the solution based on the ITAE gives the best results for the control solution based on the ACO-PI controller. It is interesting to note that this approach requires a short simulation time, unlike several other methods. On the other hand, the FLC yielded better results than the ACO-PI controller for variable wind speeds.

Appendix

The system parameters applied in the simulations are as shown below.

(a) SRG parameters:

Number of stator and rotor poles, $12/8$ (respectively); Frequency, $[F] = 50\ Hz$; DC supply voltage, $[V_{dc}] = 240\ V$; Reference current, $200\ A$; Hysteresis band, $[+10, -10]$; Mechanical load torque, $T_{\mathrm{m}} = -10$ N·m; DC link capacitor, C $3^{e-3}F$; Speed of wind, $\omega = 157\ rad/s$; Voltage of excitation, $V_{ewc} = 50\ V$; Initial voltage, $V_{CC_{init}} = 400\ V$; V_{dc} reference, $V_{CCref} = 400\ V$; Load, $R =$

1600 Ω ; Upper limit of turn-off angle, $\theta_{offmax} = 21$; Firing angle, $\theta_{on} = 40$; Maximum current ,I_{max} = 8.5 A.

(b) PI controller parameters:

The boundaries of K_p and K_i are $[0.1\ 5]$ and $[0.5\ 10]$, respectively.

(c) ACO parameters:

Number of iterations, n_n = 100; Number of ants = 30; Pheromone decay parameter, α = 0.8; Relative importance of pheromone with respect to distance, β = 0.2; Evaporation rate = 0.7; Number of parameters = 2; Number of nodes = 1000.

Conflict of interest

All authors declare no conflict of interest regarding this paper.

References

1. El-Shahat A, Hunter A, Rahman M, et al. (2019) Ultra-high speed switched reluctance motor-generator for turbocharger applications. *Energy Procedia* 162: 359–368. https://doi.org/10.1016/j.egypro.2019.04.037
2. Dias RJ, Oliveira BA, Silva KA, et al. (2020) Modelling, simulation and comparative study between switched reluctance generator 8 × 6 and switched reluctance generator 12 × 8. *Renewable Energy Power Qual J* 18: 386–390. https://doi.org/10.24084/repqj18.340
3. Fernao Pires V, Cordeiro A, Foito D, et al. (2020) A multilevel fault-tolerant power converter for a switched reluctance machine drive. *IEEE Access* 8: 21917–21931. https://doi.org/10.1109/ACCESS.2020.2967591
4. Ćalasan MP, Vujičić VP (2017) SRG converter topologies for continuous conduction operation: A comparative evaluation. *IET Electr Power Appl* 11: 1032–1042. https://doi.org/10.1049/iet-epa.2016.0659
5. Mosaad MI (2020) Direct power control of SRG-based WECSs using optimised fractional-order PI controller. *IET Electr Power Appl* 14: 409–417. https://doi.org/10.1049/iet-epa.2019.0194
6. Brouri A, Kadi L, Tounzi A, et al. (2021) Modelling and identification of switched reluctance machine inductance. *Aust J Electr Electron Eng* 18: 8–20. https://doi.org/10.1080/1448837X.2020.1866269
7. Kadi L, Brouri A, Ouannou A (2020) Frequency-geometric identification of magnetization characteristics of switched reluctance machine. *Adv Syst Sci Appl* 20: 11–26. https://doi.org/10.25728/assa.2020.20.4.839
8. Brouri A, Giri F, Ikhouane F, et al. (2014) Identification of hammerstein-wiener systems with backlash input nonlinearity bordered by straight lines, *IFAC*. https://doi.org/10.3182/20140824-6-ZA-1003.00678
9. Brouri A, Amdouri O, Chaoui FZ, et al. (2014) Frequency identification of hammerstein-wiener systems with piecewise affine input nonlinearity, *IFAC*. https://doi.org/10.3182/20140824-6-ZA-1003.00303
10. Brouri A, Kadi L, Slassi S (2017) Frequency identification of Hammerstein-Wiener systems with backlash input nonlinearity. *Int J Control Autom Syst* 15: 2222–2232. https://doi.org/10.1007/s12555-016-0312-3

11. Brouri A, Rabyi T, Ouannou A (2018) Identification of nonlinear systems with hard nonlinearity. *2018 5th Int Conf Control Decis Inf Technol CoDIT 2018,* 506–511. https://doi.org/10.1109/CoDIT.2018.8394834
12. Benyassi M, Brouri A, Rabyi T, et al. (2019) Identification of nonparametric linear systems. *Int J Mech* 13: 60–63. Available from: http://www.naun.org/main/NAUN/mechanics/2019/a142003-abz.pdf.
13. Brouri A, Rabyi T, Ouannou A (2019) Identification of nonlinear systems having hard function. *Adv Syst Sci Appl* 19: 61–74. https://doi.org/10.25728/assa.2019.19.1.632
14. Brouri A, Kadi L, Lahdachi K (2022) Identification of nonlinear system composed of parallel coupling of Wiener and Hammerstein models. *Asian J Control* 24: 1152–1164. https://doi.org/10.1002/asjc.2533
15. Brouri A, Chaoui F-Z, Giri F (2021) Identification of Hammerstein-Wiener models with hysteresis front nonlinearities. *Int J Control,* 1–15. https://doi.org/10.1080/00207179.2021.1972160
16. Brouri A (2022) Wiener-Hammerstein nonlinear system identification using spectral analysis. *Int J Robust Nonlinear Control* 32: 6184–6204. https://doi.org/10.1080/00207179.2021.1972160
17. Viajante GP, Chaves EN, Miranda LC, et al. (2021) Design and implementation of a fuzzy control system applied to a 6 × 4 SRG. *IEEE Trans Ind Appl* 57: 528–536. https://doi.org/10.1109/TIA.2020.3037263
18. Kerdtuad P, Kittiratsatcha S (2014) A novel output power control for variable-speed switched reluctance generators using artificial neural network. *2014 17th Int Conf Electr Mach Syst ICEMS 2014,* 2839–2845. https://doi.org/10.1109/ICEMS.2014.7013981
19. Li S, Zhang S, Habetler TG, et al. (2019) Modeling, design optimization, and applications of switched reluctance machines—A review. *IEEE Trans Ind Appl* 55: 2660–2681. https://doi.org/10.1109/TIA.2019.2897965
20. El-Sayed Ahmed Ibrahim H, Said Sayed Ahmed M, Mohamed Awad K (2018) Speed control of switched reluctance motor using genetic algorithm and ant colony based on optimizing PID controller. *ITM Web Conf* 16: 01001. https://doi.org/10.1051/itmconf/20181601001
21. Mosaad MI, Elkalashy NI, Ashmawy MG (2018) Integrating adaptive control of renewable distributed switched reluctance generation and feeder protection coordination. *Electr Power Syst Res* 154: 452–462. https://doi.org/10.1016/j.epsr.2017.09.017
22. Oliveira AL, Filho AJS, Di APSG, et al. (2019) P + RES controller applied to the direct power control of switched reluctance generator. *J Control Autom Electr Syst*. https://doi.org/10.1007/s40313-019-00543-1
23. Saad NH, El-Sattar AA, Metally ME (2018) Artificial neural controller for torque ripple control and maximum power extraction for wind system driven by switched reluctance generator. *Ain Shams Eng J* 9: 2255–2264. https://doi.org/10.1016/j.asej.2017.03.005
24. Nunes H, Pestana L, Mariano S, et al. (2018) Position control of linear switched reluctance machine using flower pollination algorithm. *9th Int Conf Intell Syst 2018 Theory, Res Innov Appl IS 2018-Proc,* 337–342. https://doi.org/10.1109/IS.2018.8710462
25. Hannan MA, Ali JA, Mohamed A, et al. (2018) Optimization techniques to enhance the performance of induction motor drives: A review. *Renewable Sustainable Energy Rev* 81: 1611–1626. https://doi.org/10.1016/j.rser.2017.05.240

26. Lekhchine S, Bahi T, Soufi Y (2014) Indirect rotor field oriented control based on fuzzy logic controlled double star induction machine. *Int J Electr Power Energy Syst* 57: 206–211. https://doi.org/10.1016/j.ijepes.2013.11.053
27. Joshi P, Arora S (2017) Maximum power point tracking methodologies for solar PV systems – A review. *Renewable Sustainable Energy Rev* 70: 1154–1177. https://doi.org/10.1016/j.rser.2016.12.019
28. Barros TAS, Neto PJS, Filho PSN, et al. (2016) Approach for performance optimization of switched reluctance generator in variable-speed wind generation system. *Renewable Energy* 97: 114–128. https://doi.org/10.1016/j.renene.2016.05.064
29. Shakibjoo AD, Moradzadeh M, Din SU, et al. (2021) Optimized Type-2 fuzzy frequency control for multi-area power systems. *IEEE Access* 10: 6989–7002. https://doi.org/10.1109/ACCESS.2021.3139259
30. Bouali E-T, Abid MR, Boufounas E-M, et al. (2021) Renewable energy integration into Cloud & IoT-based smart agriculture. *IEEE Access* 10: 1175–1191. https://doi.org/10.1109/access.2021.3138160
31. Ghosh S (2021) Neuro-Fuzzy-Based IoT assisted power monitoring system for smart grid. *IEEE Access* 9: 168587–168599. https://doi.org/10.1109/ACCESS.2021.3137812
32. Dang XK, Do VD, Nguyen XP (2020) Robust adaptive fuzzy control using genetic algorithm for dynamic positioning system. *IEEE Access* 8: 222077–222092. https://doi.org/10.1109/ACCESS.2020.3043453
33. Park K, Chen Z (2012) Self-tuning fuzzy logic control of a switched reluctance generator for wind energy applications. *Proc-2012 3rd IEEE Int Symp Power Electron Distrib Gener Syst PEDG 2012,* 357–363. https://doi.org/10.1109/PEDG.2012.6254026
34. Behera S, Subudhi B, Pati BB (2016) Design of PI controller in pitch control of wind turbine: A comparison of PSO and PS algorithm. *Int J Renewable Energy Res* 6: 271–281. https://doi.org/10.20508/ijrer.v6i1.3137.g6783
35. Long H, Zhang Z, Song Z, et al. (2017) Formulation and analysis of grid and coordinate models for planning wind farm layouts. *IEEE Access* 5: 1810–1819. https://doi.org/10.1109/ACCESS.2017.2657638
36. Arun S, Manigandan T (2021) Design of ACO based PID controller for zeta converter using reduced order methodology. *Microprocess Microsyst* 81: 103629. https://doi.org/10.1016/j.micpro.2020.103629
37. Barros TADS, Neto PJDS, Filho PSN, et al. (2017) An approach for switched reluctance generator in a wind generation system with a wide range of operation speed. *IEEE Trans Power Electron* 32: 8277–8292. https://doi.org/10.1109/TPEL.2017.2697822
38. Oshaba AS, Ali ES, Abd Elazim SM (2017) Speed control of SRM supplied by photovoltaic system via ant colony optimization algorithm. *Neural Comput Appl* 28: 365–374. https://doi.org/10.1007/s00521-015-2068-8

© 2022 the Author(s), licensee AIMS Press. This is an open access article distributed under the terms of the Creative Commons Attribution License (http://creativecommons.org/licenses/by/4.0)